

Skyrmion-skyrmion interaction induced by itinerant electrons in a ferromagnetic strip

E. Iroulart^{1,2} and H. D. Rosales^{1,2,3}

¹*Instituto de Física de Líquidos y Sistemas Biológicos (IFLYSIB),
UNLP-CONICET, Facultad de Ciencias Exactas, La Plata, Argentina*

²*Departamento de Física, Facultad de Ciencias Exactas,
Universidad Nacional de La Plata, La Plata, Argentina*

³*Departamento de Cs. Básicas, Facultad de Ingeniería,
Universidad Nacional de La Plata, C.C. 67, 1900 La Plata, Argentina*

(Dated: December 7, 2021)

Magnetic skyrmions are promising spin textures for building next-generation magnetic memories and spintronic devices. Nevertheless, one of the major challenges in realizing skyrmion-based devices is the stabilization of ordered arrays of these spin textures in different geometries. Here we numerically study the skyrmion-skyrmion interaction potential that arises due to the dynamics of itinerant electrons coupled to the magnetic texture in a ferromagnetic background with racetrack geometry. We consider different topological textures (ferromagnetic (FM) and antiferromagnetic (AFM)), namely: skyrmions, antiskyrmions and biskyrmions. We show that at low electron filling, for sufficiently short separation, the skyrmions strongly couple each other yielding a bound-state bound by electronic dynamics. However, when the filling is increased, the interaction potential energy presents local minima at specific values of the skyrmion-skyrmion distance. Each of these local minima correspond to energetically stable positions of skyrmions which are “protected” by well defined energy barriers. By inspecting the local charge density, we find that in the case of AFM skyrmions, the local antiferromagnetic nature prevents electronic penetration into the core, allowing the AFM skyrmions to be seen as infinite potential barriers for electrons.

I. INTRODUCTION

From the theoretical proposal in the last century and the subsequent experimental evidence in chiral magnets^{1–7}, magnetic skyrmions have garnered enormous interest due to their potential applications as promising information carriers in spintronics, including the design of racetrack memories^{8–12}. The advantages presented by skyrmions compared to other standard magnetic textures are the small currents needed for their propagation, their smaller size ($\sim 1 - 100$ nm diameter) and their topological nature which provides a significant energy barrier to avoid skyrmion annihilation¹².

Currently, there is a large family of topological skyrmion-like textures that includes the standard ferromagnetic skyrmions (FM) (Fig. 1a), antiferromagnetic skyrmions (AFM)^{13–20} (Fig. 1b), antiskyrmions²¹ (Fig. 1c), biskyrmions²² (Fig. 1d), skyrmioniums²³, ferromagnetic skyrmions^{24,25} and fractional skyrmions^{26–28}, among others (for a recent review, see for example^{29–31}). In particular, AFM skyrmions have become the subject of intense focus in the context of antiferromagnetic spintronics³². The interest in AFM skyrmions arises from the effect of coupling conduction electrons to the local magnetic background: the electrons accumulate a Berry phase as they travel through skyrmions spin configuration, which acts as a local effective magnetic field leading to topological Hall effect (THE)^{33,34} and the skyrmion Hall effect^{14,35–37}. Compared with FM skyrmions, AFM ones can move along the direction of the driving force without showing the skyrmion Hall effect. Therefore, they could be ideal information carriers for future spintronic devices, such as racetrack-type memories and logic

computing devices.

Nevertheless, potential applications concerning skyrmions or the afore-mentioned analogues demand the understanding of the inter-skyrmion interactions and the effect of the space confinement in nano-sized geometries. In regard to this problem, the pairwise interaction between ferromagnetic skyrmions has been addressed recently, focusing on interaction mediated by magnetic fluctuations in systems with much larger sizes compared to the skyrmion radius³⁸. From another side, recent theoretical studies have predicted that inter-skyrmion interaction is always repulsive and decays exponentially at a large distance³⁹, while when skyrmions are nucleated in experiments they incidentally appear close to each other. However, the analysis of the contribution of the itinerant electrons on the skyrmion-skyrmion pair interaction has not yet been explored. This raises the question of whether this contribution can have drastic consequences in relation to the geometric/spacial confinement in racetrack geometries.

This paper seeks to address the study of the itinerant electrons-induced skyrmion-skyrmion interaction in a ferromagnetic background as a function of the skyrmion-skyrmion distance dx [see Fig. 1], and the filling factor n . Through numerical calculations, we studied the influence of the skyrmion nature (both skyrmions FM or both AFM) and its topological charge Q : $Q = -1$ (skyrmion), $Q = +1$ (antiskyrmion) and $Q = -2$ (biskyrmion). The dependence of the skyrmion energy on the distance dx allows us to determine the stable positions of the skyrmions along the nanostripe. The special cases of the ferromagnetic (FM-FM) and antiferromagnetic (AFM-AFM) skyrmion-skyrmion interaction are discussed re-

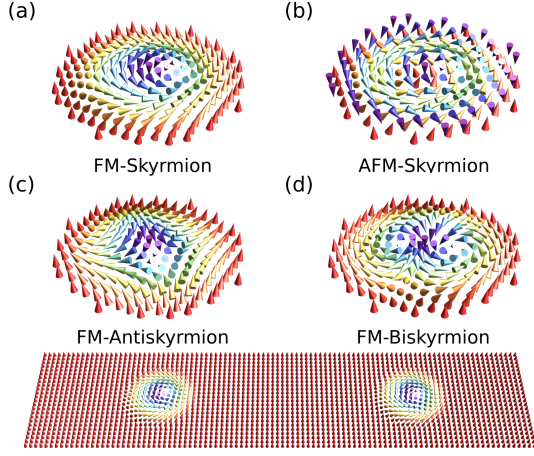


FIG. 1. (Color online) Schematics of various skyrmions; (a) ferromagnetic skyrmion, (b) antiferromagnetic skyrmion, (c) anti-skyrmion, and (d) biskyrmion. Bottom: skyrmions embedded in a collinear ferromagnetic background.

vealing a regular distribution of energy minima at specific values of separation indicating positional stability. We found that at low fillings both cases show a very close behavior developing a very similar pattern of local minima; while at higher fillings, the AFM case presents a much more regular distribution of minimums that indicates greater positional stability. In addition, we studied the local electronic charge distribution which allows us to highlight the fundamental difference between the FM and AFM cases: while in the first case, the electronic charge penetrates the core of the skyrmion as the filling increases, in the second case the antiferromagnetic nature of the magnetic texture prevents it. This allows us to view AFM skyrmions as hard disks or pseudo-particles that present greater positional stability. We found that in the AFM case, due to this characteristic the skyrmion-skyrmion problem presents a close relation with the double-well potential problem, showing quite similar energy vs dx curves. Finally, we analyzed the effect of considering skyrmions of charge $Q \neq -1$.

II. MODEL AND ANSÄTZE

To set the stage, we consider a tight binding model on a rectangular lattice of $L_x \times L_y$ sites with mixed boundary conditions, that is, periodic boundary condition along x and open boundary condition along the y -axis. The hopping term and the interaction of itinerant electrons with a magnetic texture are described by the following Hamiltonian,

$$\mathcal{H} = -t \sum_{\langle \mathbf{r}, \mathbf{r}' \rangle} \hat{c}_{\mathbf{r}, \sigma}^\dagger \hat{c}_{\mathbf{r}', \sigma} - J_H \sum_{\mathbf{r}} \mathbf{S}_{\mathbf{r}} \cdot \mathbf{s}_{\mathbf{r}} \quad (1)$$

where the operator $\hat{c}_{\mathbf{r}, \sigma}^\dagger$ ($\hat{c}_{\mathbf{r}, \sigma}$) creates (annihilates) an electron with spin $\sigma = \pm 1/2$ at site \mathbf{r} . The first term

t is the transfer integral between nearest-neighbor sites of itinerant electrons. The second term describes the Hund coupling between the spin of itinerant electrons $\mathbf{s}_{\mathbf{r}} = (1/2) \sum_{\sigma\sigma'} \hat{c}_{\mathbf{r}, \sigma}^\dagger \vec{\sigma}_{\sigma\sigma'} \hat{c}_{\mathbf{r}, \sigma'}$ and localized classical spins with coupling constant J_H , where $\vec{\sigma}$ is the vector of Pauli matrices. In the computations, we take the lattice spacing $a = 1$ and the hopping constant $t = 1$ as an energy unit.

Hereafter, let's focus in the $J_H/t \gg 1$ regime, where the spin of the hopping electron is forced to align parallel to the local moment and the low-energy physics can be described by an effective Hamiltonian of spinless fermions as

$$\mathcal{H}_{eff} = - \sum_{\langle \mathbf{r}, \mathbf{r}' \rangle} t_{\mathbf{r}\mathbf{r}'}^{eff} \hat{d}_{\mathbf{r}}^\dagger \hat{d}_{\mathbf{r}'} \quad (2)$$

where $\hat{d}_{\mathbf{r}}^\dagger$ ($\hat{d}_{\mathbf{r}}$) is the creation (annihilation) fermion operator and $t_{\mathbf{r}\mathbf{r}'}^{eff}$ is the effective transfer integral (see appendix for details).

For the purpose of studying the effective interaction between consecutive skyrmions on the racetrack geometry, we employ artificial skyrmion textures constructed using the finite size skyrmion ansatz (centered at the origin $\mathbf{r} = (x, y) \equiv (0, 0)$)⁴⁰:

$$\text{Ferromagnetic: } \mathbf{S}^{\text{FM}} = \begin{bmatrix} \sin(f) \cos(\phi) \\ \sin(f) \sin(\phi) \\ \cos(f) \end{bmatrix} \quad (3)$$

$$\text{Antiferromagnetic: } \mathbf{S}^{\text{AFM}} = (-1)^{x+y} \mathbf{S}^{\text{FM}} \quad (4)$$

where $f \equiv f(r) = (1 - r/R)\Theta(R - r)$, R is the skyrmion radius, $\Theta(R - r)$ is the Heaviside step function, $\phi \equiv \phi(\mathbf{r}) = Q \times (\arctan(y/x) + \chi)$ with χ being the helicity and Q the topological charge^{40,41}. With these ansätze it is possible to build different types of skyrmion configurations with a spacing dx between centers of two adjacent skyrmions. In the case of AFM skyrmions (Eq. 4), we have used the most simple picture where the spin texture can be visualized as a superposition of two FM skyrmions coupled antiferromagnetically⁴² (Fig. 1b). However, it should be mentioned that it is also possible to combine skyrmions on multiple sublattices^{13,17,20,27}.

After diagonalizing the electronic Hamiltonian in Eq. (2) by an unitary transformation \mathcal{U} , we compute the ground state $|GS\rangle = \prod_{\nu=1}^n |\nu\rangle$, where ϵ_ν is the energy of the ν -th electronic eigenstate, i.e. $\mathcal{H}_{eff}|\nu\rangle = \epsilon_\nu|\nu\rangle$. The ground state energy $E(dx)$ and the on-site electron density $\rho_{\mathbf{r}}$ at zero temperature for fixed separation dx (see top of Fig. 2) at a fixed filling factor n , are given by $E(dx) \equiv \langle GS | \mathcal{H}_{eff} | GS \rangle = \sum_{\nu=1}^n \epsilon_\nu$, $\rho_{\mathbf{r}_i} = \langle GS | \hat{d}_{\mathbf{r}_i}^\dagger \hat{d}_{\mathbf{r}_i} | GS \rangle = \sum_{\nu=1}^n \mathcal{U}_{\nu,i}^* \mathcal{U}_{\nu,i} + \mathcal{U}_{\nu,i+N}^* \mathcal{U}_{\nu,i+N}$.

III. CALCULATION OF THE INTERACTION POTENTIAL

In this section, we present results for systems consisting of a pair of skyrmions with radius R in a ferromag-

netic background with size $L_x \times L_y$. Thorough the rest of this work, the term “skyrmion” is used to identify the $Q = -1$ topological texture, which can be either ferromagnetic (FM) or antiferromagnetic (AFM). We have focused on the case of a skyrmion-pair with the same topological charge $\{Q, Q\} = \{-1, -1\}$ (both FM-FM and AFM-AFM cases), $R = 8$ and $\{L_x, L_y\} = \{300, 25\}$. Furthermore, we have also analyzed the situation of different topological charges: $\{Q, Q\} = \{-1, +1\}$ and $\{Q, Q\} = \{-2, -2\}$; and larger systems sizes to rule out significant finite size effects. These results allow us to predict the interaction potential between skyrmions assuming that they are displaced along the nanotrack as shown in Fig. 1.

A. FM-FM and AFM-AFM skyrmion pair interactions with $Q = -1$

Firstly, we have considered the situation of a skyrmion-pair (FM-FM and AFM-AFM) with topological charge $Q = -1$ separated by a distance dx . We have determined the interaction potential $E(dx)$ as a function of the horizontal distance between the skyrmions at fixed filling n . Figures 2 (a-h) depicts the behavior of $E(dx)$ as a function of dx and for several values of n . One can notice that at low filling factors, there is a minimum at $dx = 2 \times R$ indicating that the more favorable arrangement corresponds to locating both SKs next to each other (black arrow in Fig. 2(a)). Therefore, for sufficiently short separation skyrmions strongly couple each other yielding a bound-state bound by electronic dynamics. More remarkable is what happens when n is increased: a sequence of well-defined local minima appear at specific values of dx (black arrows in Fig. 2(b)). Each of these local minima corresponds to energetically stable distances between skyrmions which are “protected” by well defined energy barriers (dashed lines (i) and (ii)). This general scheme of local minima is observed in both cases (FM-FM and AFM-AFM pairs). However, while in the FM case, for some fillings the interaction is repulsive at short distances (Fig. 2(d-e)); in the AFM case the global minimum always occurs in the bound-state configuration (with skyrmions next to each other). This would indicate that the bound state of AFM skyrmions would be much more stable against changes in electronic filling than in the FM case.

To confirm this picture, we construct a density plot of the interaction potential with control parameters dx and n , for both cases (FM-FM and AFM-AFM, skyrmions), shown in Fig. 3. We plot the interaction potential $E(dx) - E_{min}$ (E_{min} is the minimum value of $E(dx)$ that takes a fixed n) where blue color indicates the lowest value $E(dx) - E_{min} = 0$. As it can be seen in Fig. 3 (panels left and right), both the FM and AFM skyrmions develop well defined minima at low fillings. However, when filling n is increased, in the case of FM skyrmions the local minima become irregular and diffuse (left), while in

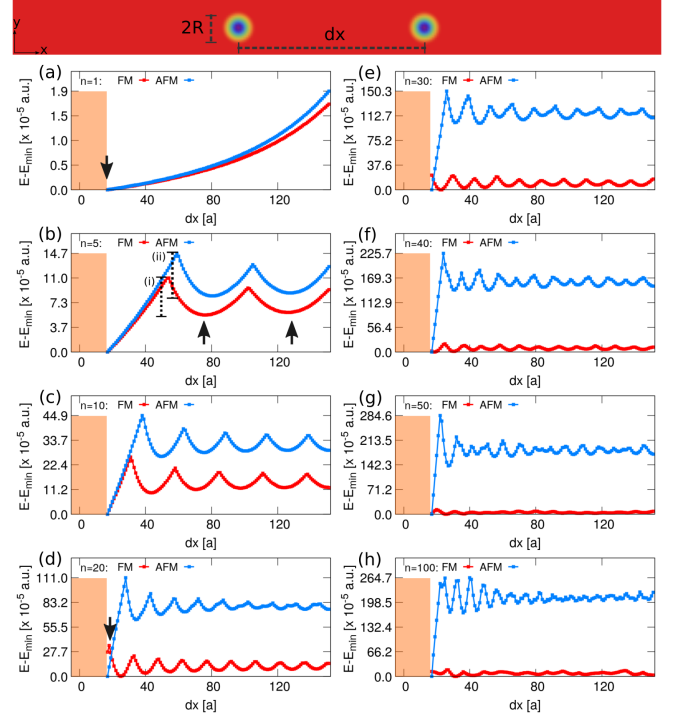


FIG. 2. (Color online) Top: An example of a skyrmion geometry performed to determine the skyrmion-skyrmion interaction potential. The length dx was progressively shortened to map out the energy increase of the system due to interactions between the skyrmions. (a)-(g) Skyrmion-skyrmion interaction potential as a function of the distance dx for different fillings: FM-FM (red) and AFM-AFM (blue).

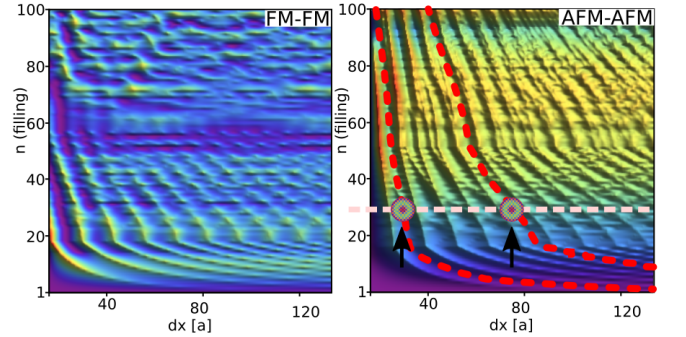


FIG. 3. (Color online) Phase diagram of the interaction potential $E(dx) - E_{min}$ as a function of the skyrmion separation dx and the filling factor n for ferromagnetic (left) and antiferromagnetic (right) skyrmions. On the right, we highlight two minimum at specific values of dx and n . Dashed red lines are a guide to the eye. Arrows indicate a possible stable (in position) skyrmion configuration.

the AFM case the minima remain well defined forming a ribbed pattern as a function of n for all cases (right). This result strongly suggests that for AFM skyrmions, the interaction with electrons generates an array of energetically stable separations of skyrmions along the track which are “protected” by well defined energy barriers

(“pinning sites”). As a consequence, the positional stability of AFM skyrmions is expected to be greater than for their FM counterpart.

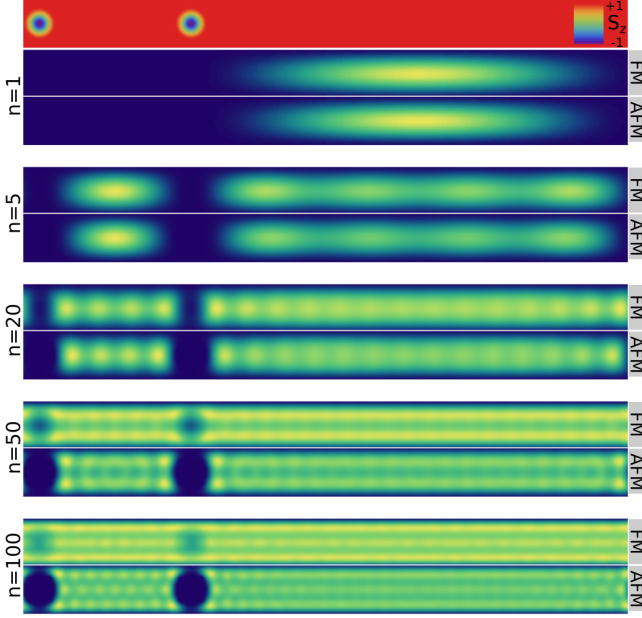


FIG. 4. (Color online) Electronic occupation in real space at different fillings and for ferromagnetic (FM) and antiferromagnetic (AFM) skyrmions configurations. For small fillings, both types of skyrmions induce a similar electronic distribution (for example for $n = 1, 5, 20$). However, as filling increases, there appears a non-zero probability that electrons will penetrate into the FM skyrmions ($n = 50, 100$). The situation is completely different in the case of AFM skyrmions where the local antiferromagnetic character of the texture generates energy barriers that prevent electronic penetration.

In order to analyze the spatial localization of the electronic states, we calculate the electronic occupation $\rho_{\mathbf{r}}$ with the model described in section II, presenting the results in Fig. 4. At the top of the figure we show the spin texture consisting of a skyrmion pair (FM-FM or AFM-AFM) separated by a distance dx . Below, we present the local electron density distributions at different n fillings for both cases. Quite remarkably, our initial observation was that for low fillings (as an example we show $n = 1, 5$), both cases present very similar distributions, showing zero electronic penetration within the skyrmion region.

However, for larger fillings ($n = 20, 50$ in Fig. 4) in the FM-FM case a non-zero local electron density can be seen inside the skyrmion region ($r < R$). This is in sharp contrast to the AFM-AFM case, where the charge density inside the skyrmion vanishes.

From a theoretical point of view, let's remember that the Berry phase, i.e. the quantum-mechanical phase picked up by electrons when their spin follows the orientation of the local magnetization $\mathbf{S}_{\mathbf{r}}$, can be rewritten as an effective Aharonov-Bohm phase $a_{\mathbf{r},\mathbf{r}'}$ associated with an “emergent” local magnetic field $B_{\mathbf{r}}^z = \frac{1}{2}\mathbf{S}_{\mathbf{r}} \cdot (\partial_x \mathbf{S}_{\mathbf{r}} \times \partial_y \mathbf{S}_{\mathbf{r}})$.

In the case of FM skyrmions we expect this effective field to have a smooth dependence with the position, while this would not necessarily be the case for AFM skyrmions. This can be verified using the ansätze of our study to calculate the effective fields for both cases, obtaining $B_{\mathbf{r}}^{z,AFM} = (-1)^{x+y} B_{\mathbf{r}}^{z,FM}$. For the AFM case, there is a rapid oscillation of the effective field, which translates into a strong barrier potential for the electrons that prevents transmission through them. This picture is maintained for different separations between skyrmions as can be seen in Fig. 5 (panel (a)) showing the electronic distribution for the case of AFM skyrmions for different values of the distance dx .

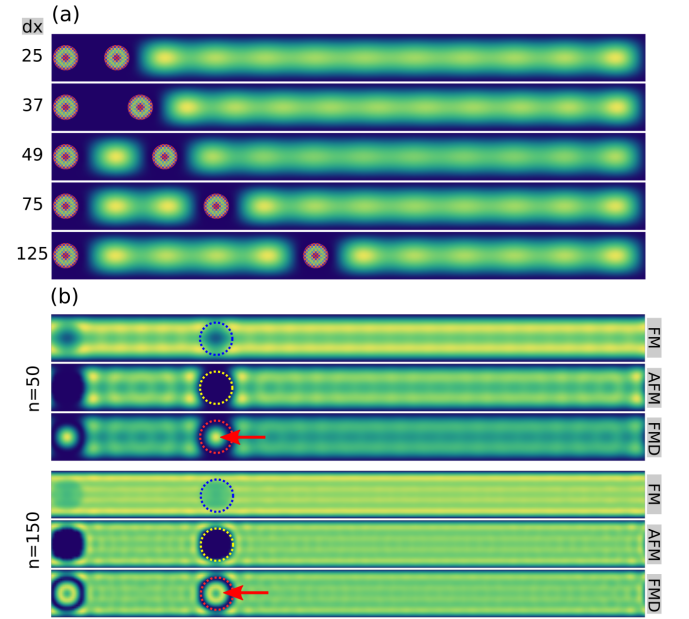


FIG. 5. (Color online) (a) Electronic occupation in real space for a filling $n = 10$ and for different skyrmion (AF) distances dx . (b) Comparison of the electronic occupation between FM-FM, AFM-AFM skyrmion pairs and pairs of ferromagnetic domains FMD-FMD (with net magnetization opposite to the external field) of equal size. It can be seen that for large fillings, electronic states appear located inside the FMD's.

It should be noted that this behavior is intrinsic to AFM skyrmions. This can be appreciated much better if we consider the electronic occupation for FM-FM, AFM-AFM skyrmions and circular homogeneous ferromagnetic domains (FMD). In Fig. 5(b) we make the comparison of the three magnetic textures for large fillings: FM-FM skyrmions have a non-zero density inside; zero penetration into its core is observed in AFM-AFM skyrmions; while in the case of FMD-FMD localized circular states are observed inside the ferromagnetic domains.

1. Analogy with the double-well potential problem

The fact that the exactly vanishing of the electronic density inside of the AFM skyrmions leads us to suppose that they can be treated as impenetrable (circular) barriers for the electrons. Therefore, we may draw a parallel between the situation of two skyrmions in a racetrack geometry with the quantum-mechanical textbook problem of a non-relativistic particle confined in infinite wells, at least when the skyrmion diameter is comparable with the width L_y . Let us recall that the electronic energies of non-relativistic free electrons of mass m in a double well (DW) configuration (see Fig. 6) are given by $E_{DW}^{(l,m)}(dx) = \left\{ \frac{Cl^2}{dx^2}, \frac{Cm^2}{(L-dx)^2} \right\}$, $l, m = 1, \dots$, $C = 2\hbar^2\pi^2/2m$. Then the energy of the system at fixed filling n is

$$E_{DW}(dx) = \sum_{l,m|l+m=n} E_{DW}^{(l,m)}(dx) \quad (5)$$

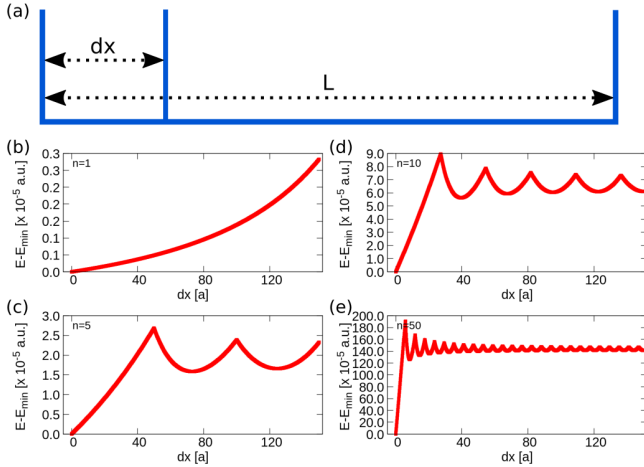


FIG. 6. (Color online) (a) Double potential well problem. In panels (b)-(e) we show the system energy as a function of the distance dx . It can be seen that the interaction potential is almost the same as that in the case of a couple of AFM skyrmions with topological charge $\{Q, Q\} = \{+1, +1\}$ in Fig. 2.

In Fig. 6(b-e) we present several curves of the interaction potential $E_{DW}(dx) - E_{min}$. One can quickly appreciate the great similarity between the energy curves in the figures 6(b-e) and the interaction potential $E(dx)$ in the case of AFM skyrmions (see Fig. 2). The presence of a global minimum at $dx = 2 \times R$ and the array of energetically stable positions (separations dx) reinforces the idea that AFM skyrmions can be seen as impenetrable barriers for the itinerant electrons.

B. FM-FM and AFM-AFM pairs: skyrmions-antiskyrmion and biskyrmion-biskyrmion interaction potential

Up to now, we have focused on FM-FM and AFM-AFM skyrmions with topological charge $Q = -1$. As a final analysis, we study the effect of introducing skyrmions with different topological charge, i.e. antiskyrmions ($Q = +1$) and biskyrmions ($Q = -2$). In order to show this, we have explicitly computed the interaction potential $E(dx)$ as a function of the horizontal distance between the FM-FM and AFM-AFM skyrmions for two specific cases: $\{Q, Q\} = \{-1, +1\}$ (skyrmion-antiskyrmion) and $\{Q, Q\} = \{-2, -2\}$ (biskyrmion-biskyrmion). First, we analyze the interaction potential $E(dx)$ for FM skyrmions is displayed in Fig. 7(a). We see that the cases $\{Q, Q\} = \{-1, -1\}$ and $\{Q, Q\} = \{-2, -2\}$ exhibit almost the same behavior. The case $\{Q, Q\} = \{-1, +1\}$ presents slight differences that arise from the opposite sign of the topological charges, although it conserves the structure of local minima observed in the other cases. In the case of AFM skyrmions (Fig. 8(a)) we obtain a perfect agreement for the three cases studied, suggesting that in the AFM case the topological charge has a much smaller effect than in the FM case.

This great similarity between the three cases of topological charges can be understood from inspection of the local field felt by electrons: B_r^z . In Figs. 7(c) and 8(c) we present the calculated effective field associated with the configurations 7(b) and 8(b) respectively. It can be seen that, except for the central site, all the distributions of B_r^z present the same structure (and opposite sign in the case $Q = +1$). This indicates that the results obtained in the case of $\{Q, Q\} = \{-1, -1\}$ are actually valid for different topological charges.

IV. CONCLUSIONS

In recent years, magnetic skyrmions have emerged as promising candidates for devices for memory and logic applications. From the experimental point of view, the skyrmions often come in close proximity with each other, opening the natural question about how this can affect their stability, motion and spacial confinement. In this regard, we have studied the itinerant electrons-induced skyrmion-skyrmion interaction in a racetrack ferromagnetic magnetic film. We have considered several situations: FM-FM and AFM-AFM skyrmions with three possible sets of topological charges: $\{Q, Q\} = \{-1, -1\}$ (skyrmion-skyrmion), $\{Q, Q\} = \{-1, +1\}$ (skyrmion-antiskyrmion) and $\{Q, Q\} = \{-2, -2\}$ (biskyrmion-biskyrmion). We found that, at low filling factors, both the FM and AFM skyrmions develop well defined array of energetically stable separations of skyrmions along the track which are “protected” by well defined energy barriers. However, when filling n is increased, in the case

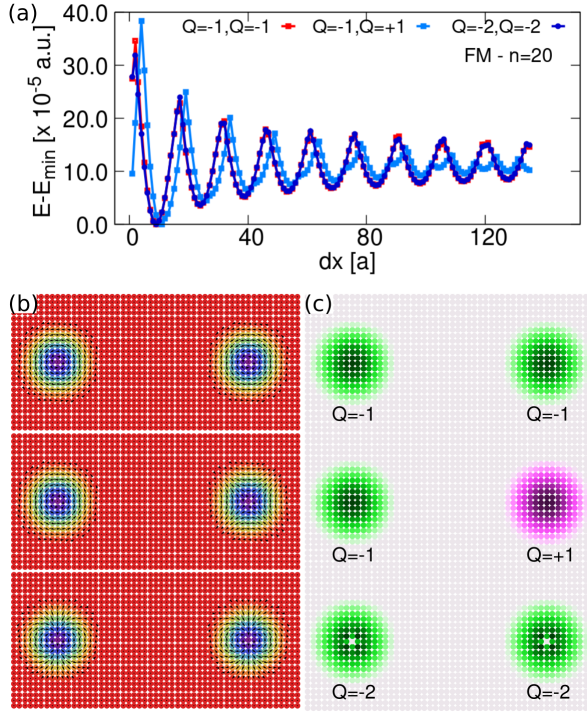


FIG. 7. (Color online) (a) Interaction potential $E(dx)$ as a function of the horizontal distance between the FM skyrmions with topological charge $\{Q, Q\} = \{-1, -1\}$ (red), $\{Q, Q\} = \{-1, +1\}$ (cyan) and $\{Q, Q\} = \{-2, -2\}$ (blue); (b) magnetic texture and (c) the calculated topological charge density.

of FM skyrmions the local minimums become irregular and diffuse, while in the AFM case the minimums remain well defined forming a ribbed pattern as a function of n for all cases. These minimums in energy act as effective “pinning sites” along the racetrack, i.e., preferred positions for the skyrmions along the track. In addition, we have investigated the electronic distribution occupation. We found that at low fillings, both cases (FM- and AFM-skyrmions), the electronic local density states reside outside the skyrmion region, showing zero electronic penetration within the skyrmion region. However, for larger fillings, in the FM case a non-zero local electron density emerges inside skyrmion core. This is in sharp contrast to the AFM case even for large fillings showing that the AFM character of the skyrmions has a very large energy cost on the itinerant electrons inside the skyrmion region.

We have confirmed that these results are valid even for other configurations of the topological $Q \neq 1$. In order to show this, we have explicitly computed the interaction potential $E(dx)$ as a function of the horizontal distance between the FM and AFM skyrmions for two specific cases: $\{Q, Q\} = \{-1, +1\}$ and $\{Q, Q\} = \{-1, -1\}$. As a general result, we found that for FM skyrmions, the cases $\{Q, Q\} = \{-1, -1\}$ and $\{Q, Q\} = \{-2, -2\}$ exhibit almost the same behavior while the case $\{Q, Q\} = \{-1, +1\}$ presents slight differences that arise from the

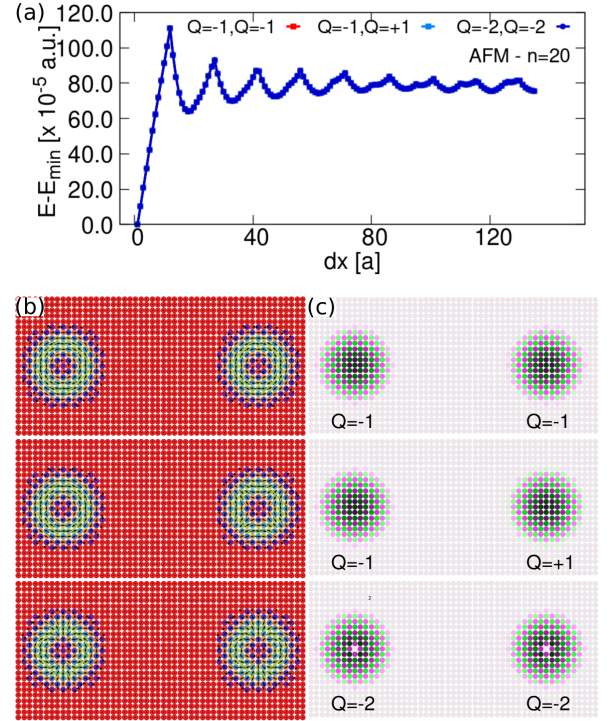


FIG. 8. (Color online) (a) Potential interaction $E(dx)$ as a function of the horizontal distance between the AFM skyrmions with topological charge $\{Q, Q\} = \{-1, -1\}$ (red), $\{Q, Q\} = \{-1, +1\}$ (cyan) and $\{Q, Q\} = \{-2, -2\}$ (blue); (b) magnetic texture and (c) the calculated topological charge density.

opposite sign of the topological charge, although it conserves the structure of local minimums observed in the other cases. In the case of AFM skyrmions we observed a perfect agreement for the three cases studied, suggesting that in the AFM case the topological charge has a much smaller effect than in the FM case. Therefore, our results support the idea that AFM skyrmions are good candidates for electronic devices.

V. ACKNOWLEDGMENTS

This work was partially supported by CONICET (PIP 2021-11220200101480CO) and SECyT-UNLP (I+D X893). H.D.R. thanks Flavia Gómez Albarracín for valuable comments.

Appendix: Effective Hamiltonian Derivation

We consider a Kondo lattice model on the square lattice where the itinerant electrons are coupled with the classical magnetic moments by a Hund’s coupling as

$$\mathcal{H} = -t \sum_{\langle \mathbf{r}, \mathbf{r}' \rangle, \sigma} (\hat{c}_{\mathbf{r}\sigma}^\dagger \hat{c}_{\mathbf{r}', \sigma} + \text{h.c.}) - J_H \sum_{\mathbf{r}} \mathbf{S}_{\mathbf{r}} \cdot \mathbf{s}_{\mathbf{r}} \quad (\text{A.1})$$

where $\hat{c}_{\mathbf{r}\sigma}$ ($\hat{c}_{\mathbf{r}\sigma}^\dagger$) is the creation (annihilation) operator at the site \mathbf{r} with spin ($\sigma = \pm 1/2$), t is the hopping amplitude between nearest-neighbor sites, J_H is the Hund's coupling strength between the electron spin $\mathbf{s}_{\mathbf{r}} = \frac{1}{2}\hat{\mathbf{c}}_{\mathbf{r},\mu}^\dagger \vec{\sigma}^{\mu\nu} \hat{c}_{\mathbf{r},\nu}$ and the local magnetic moment $\mathbf{S}_{\mathbf{r}}$. In the strong Hund coupling limit $J_H \gg t$, the spin of the itinerant electron is fully aligned with magnetic moment $\mathbf{S}_{\mathbf{r}}$. Therefore, it is trivial to observe that the electronic spectrum splits into a low- and high-energy band set^{34,43}.

In order to obtain an effective Hamiltonian describing the low energy sector we choose the quantization axis in the site \mathbf{r} pointing along the direction of the local magnetization, so we introduce the unitary transformation \mathcal{U} between the fermionic operators, $\hat{c}_{\mathbf{r}}^\dagger = \{\hat{c}_{\mathbf{r}\uparrow}^\dagger, \hat{c}_{\mathbf{r}\downarrow}^\dagger\}$ and $\hat{f}_{\mathbf{r}}^\dagger = \{\hat{f}_{\mathbf{r}\uparrow}^\dagger, \hat{f}_{\mathbf{r}\downarrow}^\dagger\}$, such that $\hat{c}_{\mathbf{r}} = \mathcal{U}_{\mathbf{r}} \cdot \hat{f}_{\mathbf{r}}$ and $\mathcal{U}_{\mathbf{r}}^\dagger \cdot (\mathbf{S}_{\mathbf{r}} \cdot \vec{\sigma}) \cdot \mathcal{U}_{\mathbf{r}} =$

σ_z . The general expression of the matrix transformation is given by

$$\mathcal{U}_{\mathbf{r}}^\dagger = \mathbf{m}_{\mathbf{r}} \cdot \vec{\sigma} = \begin{pmatrix} \cos \frac{\theta_{\mathbf{r}}}{2} & \sin \frac{\theta_{\mathbf{r}}}{2} e^{-i\phi_{\mathbf{r}}} \\ \sin \frac{\theta_{\mathbf{r}}}{2} e^{i\phi_{\mathbf{r}}} & -\cos \frac{\theta_{\mathbf{r}}}{2} \end{pmatrix},$$

where vector $\mathbf{m}_{\mathbf{r}} = \{\sin \frac{\theta_{\mathbf{r}}}{2} \cos \phi_{\mathbf{r}}, \sin \frac{\theta_{\mathbf{r}}}{2} \sin \phi_{\mathbf{r}}, \cos \frac{\theta_{\mathbf{r}}}{2}\}$ is defined from the local magnetic moment $\mathbf{S}_{\mathbf{r}} = (\cos \phi_{\mathbf{r}} \sin \theta_{\mathbf{r}}, \sin \phi_{\mathbf{r}} \sin \theta_{\mathbf{r}}, \cos \theta_{\mathbf{r}})$. With all this, the transformed Hamiltonian reads

$$\mathcal{H} = -t \sum_{\mathbf{r}\mathbf{r}'} \hat{f}_{\mathbf{r}}^\dagger \mathcal{U}_{\mathbf{r}}^\dagger \mathcal{U}_{\mathbf{r}'} \hat{f}_{\mathbf{r}'} - J_H \sum_{\mathbf{r}} \hat{f}_{\mathbf{r}}^\dagger \sigma^{(z)} \hat{f}_{\mathbf{r}} \quad (\text{A.2})$$

where

$$\mathcal{U}_{\mathbf{r}}^\dagger \mathcal{U}_{\mathbf{r}'} = \begin{pmatrix} \cos \frac{\theta_{\mathbf{r}}}{2} \cos \frac{\theta_{\mathbf{r}'}}{2} + \sin \frac{\theta_{\mathbf{r}}}{2} \sin \frac{\theta_{\mathbf{r}'}}{2} e^{-i(\phi_{\mathbf{r}} - \phi_{\mathbf{r}'})} & \cos \frac{\theta_{\mathbf{r}}}{2} \sin \frac{\theta_{\mathbf{r}'}}{2} e^{-i\phi_{\mathbf{r}'}} - \cos \frac{\theta_{\mathbf{r}'}}{2} \sin \frac{\theta_{\mathbf{r}}}{2} e^{-i\phi_{\mathbf{r}}} \\ \cos \frac{\theta_{\mathbf{r}'}}{2} \sin \frac{\theta_{\mathbf{r}}}{2} e^{i\phi_{\mathbf{r}}} - \cos \frac{\theta_{\mathbf{r}}}{2} \sin \frac{\theta_{\mathbf{r}'}}{2} e^{i\phi_{\mathbf{r}'}} & \cos \frac{\theta_{\mathbf{r}}}{2} \cos \frac{\theta_{\mathbf{r}'}}{2} + \sin \frac{\theta_{\mathbf{r}}}{2} \sin \frac{\theta_{\mathbf{r}'}}{2} e^{i(\phi_{\mathbf{r}} - \phi_{\mathbf{r}'})} \end{pmatrix}.$$

In the strong coupling regime $J_H \gg t$, the low-energy sector can be described by effective spinless fermions: $\{\hat{a}_{\mathbf{r}}, \hat{d}_{\mathbf{r}}^\dagger\}$. As a result, the effective Hamiltonian of the system is

$$\mathcal{H}_{eff} = -t \sum_{\langle \mathbf{r}\mathbf{r}' \rangle} \cos \left(\frac{\theta_{\mathbf{r}\mathbf{r}'}}{2} \right) e^{ia_{\mathbf{r}\mathbf{r}'}} \hat{d}_{\mathbf{r}}^\dagger \hat{d}_{\mathbf{r}'}$$

where $\hat{d}_{\mathbf{r}}^\dagger$ ($\hat{d}_{\mathbf{r}}$) corresponds to the up component of $\hat{f}_{\mathbf{r}}^\dagger$ ($\hat{f}_{\mathbf{r}}$),

where $\cos \theta_{\mathbf{r}\mathbf{r}'} = \mathbf{S}_{\mathbf{r}} \cdot \mathbf{S}_{\mathbf{r}'}$ and $a_{\mathbf{r}\mathbf{r}'}$ the phase accumulated by the hopping electron,

$$a_{\mathbf{r}\mathbf{r}'} = \arctan \left(\frac{-\sin(\phi_{\mathbf{r}} - \phi_{\mathbf{r}'})}{\cos(\phi_{\mathbf{r}} - \phi_{\mathbf{r}'}) + \cot \left(\frac{\theta_{\mathbf{r}}}{2} \right) \cot \left(\frac{\theta_{\mathbf{r}'}}{2} \right)} \right).$$

-
- ¹ S. Mühlbauer, B. Binz, F. Jonietz, C. Pfleiderer, A. Rosch, A. Neubauer, R. Georgii, and P. Böni, *Science* **323**, 915 (2009).
 - ² W. Münzer, A. Neubauer, T. Adams, S. Mühlbauer, C. Franz, F. Jonietz, R. Georgii, P. Böni, B. Pedersen, M. Schmidt, *et al.*, *Physical Review B* **81**, 041203 (2010).
 - ³ X. Yu, Y. Onose, N. Kanazawa, J. Park, J. Han, Y. Matsui, N. Nagaosa, and Y. Tokura, *Nature* **465**, 901 (2010).
 - ⁴ Yu, X., Kanazawa, N., Onose, Y. *et al.* *Nature Materials* **10**, 106-109 (2011).
 - ⁵ Heinze, S., von Bergmann, K., Menzel, M. *et al.* *Nature Physics* **7**, 713-718 (2011).
 - ⁶ S. Seki, X. Yu, S. Ishiwata, and Y. Tokura, *Science* **336**, 198 (2012).
 - ⁷ A. B. Butenko, A. A. Leonov, U. K. Röbler, and A. N. Bogdanov, *Physical Review B* **82**, 052403 (2010).
 - ⁸ Fert, A., Cros, V. and Sampaio, J. *Skyrmions on the track.* *Nature Nanotechnology* **8**, 152-156 (2013).
 - ⁹ X. Zhang, Y. Zhou, M. Ezawa, G. Zhao, and W. Zhao, *Scientific Reports* **5**, 1 (2015).
 - ¹⁰ S.H. Guan and Y. Yang and Z. Jin and T.T. Liu and Y. Liu and Z.P. Hou and D.Y. Chen and Z. Fan and M. Zeng and X.B. Lu and X.S. Gao and M.H. Qin and J.-M. Liu, *Journal of Magnetism and Magnetic Materials* **546**, 168852 (2022).
 - ¹¹ V. L. Carvalho-Santos, M. A. Castro, D. Salazar-Aravena, D. Laroze, R. M. Corona, S. Allende, and D. Altbir, *Applied Physics Letters* **118**, 172407 (2021).
 - ¹² X. Zhang, Y. Zhou, K. M. Song, T.-E. Park, J. Xia, M. Ezawa, X. Liu, W. Zhao, G. Zhao, and S. Woo, *Journal of Physics: Condensed Matter* **32**, 143001 (2020).
 - ¹³ H. D. Rosales, D. C. Cabra, and P. Pujol, *Physical Review B* **92**, 214439 (2015).
 - ¹⁴ J. Barker and O. A. Tretiakov, *Physical Review Letter* **116**, 147203 (2016).
 - ¹⁵ S. A. Osorio, H. D. Rosales, M. B. Sturla, and D. C. Cabra, *Physical Review B* **96**, 024404 (2017).
 - ¹⁶ S. A. Osorio, M. B. Sturla, H. D. Rosales, and D. C. Cabra, *Physical Review B* **100**, 220404(R) (2019).
 - ¹⁷ M. E. Villalba, F. A. Gómez Albarracín, H. D. Rosales, and D. C. Cabra, *Physical Review B* **100**, 245106 (2019).
 - ¹⁸ W. Legrand, D. Maccariello, F. Ajéjas, S. Collin, A. Vecchiola, K. Bouzehouane, N. Reyren, V. Cros, and A. Fert, *Nature Materials* **19**, 34 (2020).
 - ¹⁹ Z. Liu and H. Yang, *Physica E: Low-dimensional Systems and Nanostructures* **135**, 114978 (2022).
 - ²⁰ A. Mukherjee, D. S. Kathyat, and S. Kumar, *Scientific Reports* **11**, 1 (2021).

- ²¹ A. K. Nayak, V. Kumar, T. Ma, P. Werner, E. Pippel, R. Sahoo, F. Damay, U. K. Rößler, C. Felser, and S. S. Parkin, *Nature* **548**, 561 (2017).
- ²² Yu, X., Tokunaga, Y., Kaneko, Y. *et al.* *Nature Communications* **5**, 3198 (2014).
- ²³ A. G. Kolesnikov, M. E. Stebliy, A. S. Samardak, and A. V. Ognev, *Scientific Reports* **8**, 1 (2018).
- ²⁴ S. Woo, K. M. Song, X. Zhang, Y. Zhou, M. Ezawa, X. Liu, S. Finizio, J. Raabe, N. J. Lee, S.-I. Kim, *et al.* *Nature Communications* **9**, 1 (2018).
- ²⁵ Wu, Hao and Groß, Felix and Dai, Bingqian and Lujan, David and Razavi, Seyed Armin and Zhang, Peng and Liu, Yuxiang and Sobotkiewich, Kemal and Förster, Johannes and Weigand, Markus, *et al.*, *Advanced Materials* **32**, 2003380 (2020).
- ²⁶ S.-Z. Lin, A. Saxena, and C. D. Batista, *Physical Review B* **91**, 224407 (2015).
- ²⁷ S. Gao, H. D. Rosales, F. A. Gómez Albarracín, V. Tsurkan, G. Kaur, T. Fennell, P. Steffens, M. Boehm, P. Čermák, A. Schneidewind, E. Ressouche, D. C. Cabra, C. Rüegg, and O. Zaharko, *Nature* **586**, 37-41 (2020).
- ²⁸ Z. Wang, Y. Su, S.-Z. Lin, and C. D. Batista, *Physical Review B* **103**, 104408 (2021).
- ²⁹ Y. Zhou, *National Science Review* **6**, 210 (2019).
- ³⁰ C. Back, V. Cros, H. Ebert, K. Everschor-Sitte, A. Fert, M. Garst, T. Ma, S. Mankovsky, T. Monchesky, M. Mostovoy, *et al.*, *Journal of Physics D: Applied Physics* **53**, 363001 (2020).
- ³¹ B. Göbel, I. Mertig, and O. A. Tretiakov, *Physics Reports* (2020).
- ³² T. Jungwirth, X. Marti, P. Wadley, and J. Wunderlich, *Nature Nanotechnology* **11**, 231 (2016).
- ³³ H. D. Rosales, F. A. Gómez Albarracín, and P. Pujol, *Physical Review B* **99**, 035163 (2019).
- ³⁴ M. Tomé and H. D. Rosales, *Physical Review B* **103**, L020403 (2021).
- ³⁵ G. Chen, *Nature Physics* **13**, 112 (2017).
- ³⁶ X. Zhang, Y. Zhou, and M. Ezawa, *Scientific reports* **6**, 24795 (2016).
- ³⁷ C. Jin, C. Song, J. Wang, and Q. Liu, *Applied Physics Letters* **109**, 182404 (2016).
- ³⁸ D. Capic, D. A. Garanin, and E. M. Chudnovsky, *Journal of Physics: Condensed Matter* **32**, 415803 (2020).
- ³⁹ R. Brearton, G. van der Laan, and T. Hesjedal, *Physical Review B* **101**, 134422 (2020).
- ⁴⁰ S. A. Osorio, M. B. Sturla, H. D. Rosales, and D. C. Cabra, *Physical Review B* **99**, 064439 (2019).
- ⁴¹ A. N. Bogdanov and D. Yablonskii, *Zh. Eksp. Teor. Fiz* **95**, 178 (1989).
- ⁴² S. A. Díaz, J. Klinovaja, D. Loss, and S. Hoffman, *arXiv preprint arXiv:2102.03423* (2021).
- ⁴³ K. Ohgushi, S. Murakami, and N. Nagaosa, *Physical Review B* **62**, R6065 (2000).